Two-dimensional prediction of the interface of geological formations: a comparative study

Xiaohui Qi[1, 2], Hao Wang[2], Jian Chu[2]*, Kiefer Chiam[3]

[1]Department of Mechanical and Construction Engineering, Northumbria University, Newcastle Upon Tyne, NE1 8ST, UK

[2]School of Civil and Environmental Engineering, Nanyang Technological University, 639798, Singapore

[3]Building and Construction Authority, 200 Braddell Road, 579700, Singapore

* Corresponding author

E-mail addresses: xiaohui.qi@northumbria.ac.uk (X. Qi), wang.hao@ntu.edu.sg (H. Wang), cjchu@ntu.edu.sg (J. Chu), Kiefer_CHIAM@bca.gov.sg (K. Chiam)

Abstract: The location of the interface of geological formations is an important piece of information for tunneling construction. As site investigation data are usually limited, the uncertainties in locating geological interfaces for the sections between boreholes can be large and challenging to estimate. A suitable geostatistical method is thus needed for spatial prediction of the geological interfaces. In this paper, the performance of three commonly used spatial prediction methods, namely the multivariate adaptive spline regression (MARS), conditional random field (CRF) method, and thin-plate spline interpolation (TPSI) methods, are evaluated for two-dimensional cases using the boreholes data from three sites in Singapore. The prediction accuracies, patterns of the predicted surfaces, and prediction uncertainties obtained from the three methods are compared. A zonation is also proposed to improve the prediction accuracy of the MARS method. The results indicate that the MARS method can show the spatial trend of the geological interface more clearly than the other two methods. The TPSI method produces undesirable oscillations of the surface of geological interfaces and the CRF method may underestimate the extreme values of the geological interface elevations. In general, the prediction accuracy of the MARS method is similar to that of the CRF method, but higher than that of the TPSI method. For cases with very limited data in geologically complex areas, the MARS may have larger errors than

the CRF method. However, the accuracy of the former can be significantly improved if a reasonable zonation is performed.

Keywords: Geological interface, rockhead, spatial prediction, multivariate adaptive regression spline, Bayesian-based conditional random field, thin-plate spline interpolation

1. Introduction

In tunneling constructions, engineers usually need to know the location of the interface of geological layers such as the interface between soil and rock or the so-called rockhead (Zheng et al. 2021, Li et al. 2021). This is because when different geological formations with distinctly different geotechnical properties are encountered, different excavation or support methods may be required. Due to complex tectonic and environmental factors, the location of the geological interface often has a large spatial variability (e.g., Qi et al. 2020a, b). Moreover, the available site investigation data providing information on the geological interfaces are sometimes not sufficient or lacking due to the early termination of the boreholes. For example, in engineering practices, the boreholes are customarily drilled at a spacing of 30 to 60 m or larger. It is a challenging task to accurately identify the geological interfaces in the zones between boreholes.

Various methods have been developed to interpolate the geological interfaces. These methods can be classified into two groups according to the ability to quantify the prediction uncertainty, i.e., the deterministic method and probabilistic method. Examples of the former include the inverse distance weighting method, spline interpolation, and triangulated irregular network (e.g., Lark et al. 2013, Aswar and Ullagaddi 2017), non-uniform rational basis spline fitting, and neural networks. The disadvantage of this category of methods is that it cannot provide any confidence interval for the prediction. Although it is possible to know the general accuracy of these methods through a process called cross-validation, the error from the cross-validation depends on the selection of training data. Also, the cross-validation cannot reasonably address the issue of non-stationary errors, that is, the errors in various locations such as in geologically complex areas and geologically more uniform areas may be quite different. As a result, attention has been gradually shifted to the probabilistic methods such as the Bayesian-based conditional random field method

(e.g., Qi and Liu 2019a), the kriging method (e.g., Dasaka and Zhang 2012), coupled Markov chain method (Elfeki and Dekking 2001, Li D et al. 2016, Qi et al. 2016, Deng et al. 2017), Markov random field method (Wang H et al. 2017, Wang X et al. 2018) and Bayesian compressive method (Wang and Zhao 2016, 2017, Wang Y et al. 2017, Zhao et al. 2018). The kriging method and conditional random field (CRF) method can consider the spatial variability information of a considered parameter but require a large number of data to estimate the random field parameters or semi-variogram parameters, as pointed out by Qi and Liu (2019b). The coupled Markov chain method does not need large quantities of data. Nevertheless, the method is applicable only to cases where the transition of different types of soil or geological layers possesses a Markovian property (Qi et al. 2016). The Markov random field method is capable of modeling complex geological structures. But some parameters of the method lack clear physical meanings, as pointed out by Mariethoz and Caers (2014). The recently proposed Bayesian compressive sampling method is versatile as it can model both stationary and non-stationary random fields and deal with both one-dimensional and multiple-dimensional problems (Montoya-Noguera et al. 2019, Wang Y et al. 2018, 2019, Wang Y et al. 2020, Zhao and Wang 2020). A potential problem of the method is that it is not robust when the number of measurements is much smaller than the length of the discrete signal or when the measurement noise is relatively large, as discussed in Huang et al. (2014).

To overcome these limitations, Qi et al. (2020a) have proposed to use the multivariate adaptive regression spline (MARS) method to spatially predict the location of the geological interface. The MARS is a non-parametric regression method and can automatically model the nonlinear relations between independent parameters and a response parameter. This method has been widely applied to geotechnical engineering such as pile problems (e.g., Zhang and Goh 2016, Zhang et al. 2019), slope problems (e.g., Wang L et al. 2020), and tunnel problems (e.g., Zhang et

al. 2020). For the prediction of geological interfaces, Qi et al. (2020a) illustrated that the method can provide a reasonable prediction interval that reasonably reflects the data density and geological complexity. However, the performance of the MARS relative to other spatial prediction methods is not well understood. Most comparative studies (e.g., Samui et al. 2015, Zhang and Goh 2016, Zhang et al. 2019) only focused on the prediction accuracy and ignore some important aspects such as the prediction uncertainty. Although Qi et al. (2020b) compared the spline regression method with other methods, the study focused only on one-dimensional problems.

This study compares the performance of the MARS method with another two commonly used spatial prediction methods, namely the CRF method and the thin-plate spline interpolation (TPSI) method. The CRF method is a geostatistical method and is analysed as it can also quantify the prediction uncertainty. The TPSI is a deterministic method and is considered because similar to the MARS method, it also uses spline functions. The performances, including prediction accuracies, patterns of predicted surfaces, and prediction uncertainties of various methods in dealing with two-dimensional problems are compared through a cross-validation procedure. The pattern of the predicted surface determines whether the surface is realistic while prediction uncertainty controls how much confidence should be assigned to the predicted surfaces. These aspects are rarely considered in previous studies. Borehole data from three sites located in Singapore and with different geological formations are analyzed. Site 1 reveals the interface of Kallang Formation (KF) and Old Alluvium (OA) while Sites 2 and 3 reveal the rockhead of an igneous rock formation, Bukit Timah Granite (BTG). Herein the rockhead is taken as the interface of the soil layer and rock layer in a rock formation. It is worth noting that the study also proposes to perform a zonation for the MARS method, which is rarely seen in previous applications of the MARS method.

2. Methods

The section first briefly introduces the MARS method used in the comparative study. A zonation is proposed in this subsection to improve the prediction accuracy of the MARS method. The CRF method can be found in Li X et al. (2016), Lo and Leung (2017), and Qi et al. (2020b) while the TPSI method can be found in Harder and Desmarais 1972, Duchon (1977), and MathWorks (2014). These two methods are not repeated herein. Afterward, a cross-validation procedure is used for evaluating the accuracy of various methods.

2.1 MARS and Zonation

The MARS method is a well-established non-parametric regression method, which can automatically model the nonlinear relation between predictors (independent parameters) and a response (dependent parameter). The method can be regarded to be a generalization of the piecewise polynomial regression. The built MARS model is a continuous piecewise polynomial function of the predictors, which depicts how the mean trend of the response varies with the predictors. The trend can be linear or nonlinear, depending on the order of the adopted spline basis functions. The connection point where two neighboring pieces of polynomial function meet is called a knot. The basic idea of the MARS method is determining a suitable number of knots to maximize the prediction accuracy. Unlike a linear regression which just considers the fitting error, the MARS method finds out the optimal number and location of knots through *k*-fold cross-validations. To be specific, the whole data are divided into *k* groups and each group is successively used as testing data to evaluate the prediction errors. The number of knots that correspond to the minimum averaged prediction error of the testing data is taken to be the optimal number of knots. In addition, the MARS method can also quantify the prediction uncertainty, especially non-stationary prediction uncertainty where the various areas have different levels of prediction errors.

More information on the prediction uncertainty can be found in Qi et al. (2020a). Details of the MARS method can be found in Friedman (1991), Hastie et al. (2008), and Zhang and Goh (2016).

It is worth noting that the variability of the location of a geological interface can be quite large, especially when geological structures such as faults or folds exist. The data points nearby these geologically complex areas are quite different from the data in geologically more uniform areas and the former can be considered to be outliers of the latter. When the available data are limited and the outliers are used together with the normal data for regression analyses, a misleading geological surface will be obtained. Under this condition, a zonation can be performed. The idea of the zonation is to find out the partition line between areas with significantly different spatial trends of geological interface and the data within different zones are separately used for regression analyses. The zonation ensures that the data used for regression do not contain any outliers. Ideally, if information regarding geological structures is available, the zonation can be performed according to the locations of geological structures, such as placing the partition lines of various zones along the strike of the faults. If the geological structure information is not available, one can visually inspect the areas with sharp variations of geological intervals and then place partition lines to differentiate the data with distinct differences in the elevations of geological interfaces. Multiple partition lines might be necessary if one line is not sufficient to differentiate the data. Furthermore, different zonation schemes can be tried if it is difficult to determine the locations of the partition line and the optimal one can be chosen by finding out the scheme with minimum prediction errors in cross-validations. To facilitate understandings, a flowchart of the zonation is plotted in Fig. 1.

2.2 Cross-validation

In this paper, the prediction accuracies of various spatial prediction methods are compared using a cross-validation procedure. In cross-validation, certain percentages of data are randomly drawn

as the training data while the remainder as testing data. The accuracy is denoted by two indexes, root mean squared error, *RMSE* and root mean squared relative error, *RMSRE*, as shown by

$$RMSE = \sqrt{\frac{1}{N_p}\sum_{i=1}^{N_p}(E_i - \hat{E}_i)^2} \tag{1a}$$

$$RMSRE = \sqrt{\frac{1}{N_p}\sum_{i=1}^{N_p}(\frac{E_i - \hat{E}_i}{D_i})^2} \tag{1b}$$

where N_p is the number of points in the testing group; E_i is the observed value of the geological interface elevation for the *i*th testing borehole; $\hat{E}_i$ is the predicted value of the geological interface elevation for the *i*th testing borehole and D_i is the depth of the geological interface at the *i*th testing borehole. Herein, the depth is the difference value between the elevation of the ground surface and that of the geological interface. Depth rather than elevation is used in the denominator of Eq. 1(b) because sometimes the observed elevation of the geological interface is close to zero.

3. Borehole data and geology at the three sites

Borehole data collected from three sites in Singapore are used for the comparative study. These three sites are Site 1 for an integrated metro and bus depot project at Upper Changi Road, Site 2 for a residential project at Canberra Link, Sembawang and Site 3 for a downtown metro line project and a project involving widening the Kranji Expressway at Woodland. The borehole data were extracted from site investigation reports of the three sites. However, only boreholes that have reached the rockhead or interface of KF-OA were used. Typical geological profiles at the three sites are shown in Figs. 2(a, b, c), respectively. The geological profiles were extracted from a 3D geological model constructed by geologists using a 3D geological modeling software, Subsurface Viewer, (Armstrong 2012). As shown, the main geological interfaces at the three sites are the KF – OA interface at Site 1 and the rockhead of BTG at Sites 2 and 3. The KF and OA are two deposit

167 formations formed from the late Pleistocene to the present and Plio-Pleistocene, respectively (Pitts
168 1984; Sharma et al. 1999). The former consists mainly of soft marine clay, loose alluvial muddy
169 sand, loose beach sand, soft peaty and organic mud, and coral. This formation is distributed around
170 river valleys, river mouths, river plains, coastal and offshore areas. The KF represents poor ground
171 conditions for excavation and foundation works. The Ka and Km in Fig. 2(a) denote the alluvial
172 member and marine member of the KF, respectively. The OA comprises primarily dense to
173 cemented muddy sand and gravel, which were brought down by close-connected rivers and
174 deposited in a deep basin located on the eastern Singapore Island (Chiam et al. 2003). The OA
175 generally has good geotechnical properties and is one of the major sources of sand used as fill
176 materials for land reclamations. For the safety of construction activity, it is also important to
177 identify the location of the interface of these two formations. The BTG is an igneous rock
178 formation developed in the early to middle Triassic period. It contains a variety of acid rocks
179 including granite, adamellite, granodiorite, and acid and intermediate hybrids. The BTG underlies
180 around one-third of Singapore Island and is the base rock of Singapore. The intact rock of Bukit
181 Timah Granite has high strength and is suitable for cavern construction. However, due to the
182 tectonic plate movements, the humid tropical weather, and other environmental factors in
183 Singapore, the BTG has experienced intensive weathering, leading to highly variable rockhead
184 profiles. There is also a need to identify the location of the relatively unweathered or fresh rock
185 layer of the Bukit Timah Granite. The detailed information for the three formations can be found
186 in Pitts (1984) and Sharma et al. (1999). Note that the elevation used in this study is the height
187 relative to the mean sea level determined by the tide gauge at Victoria Dock in Singapore from
188 1935 to 1937.

189 The geological interface data from boreholes at the three sites are plotted in Figs. 2(d, e, f),
190 respectively. In each figure, a surface of the geological interface is plotted along with the data
191 points. These surfaces are obtained by linear interpolations using the 'fit' function in MATLAB.
192 In total, 154, 135, and 47 data points are distributed at the three sites, which are around 1200 m ×
193 400 m, 550 m × 350 m, and 500 × 1000 in size, respectively. The data points at site 3 were limited
194 because limited boreholes were drilled in the direction perpendicular to the metro line direction.
195 The KF-OA interface elevation of the 154 boreholes ranges from −27.0 m to −1.4 m, while the
196 rockhead elevation for the boreholes at Sites 2 and 3 ranges from −50.8 m to 3.6 m, and – 38.8 m
197 to 25.3 m, respectively. The standard deviations of the geological interface elevation at the three
198 sites are 4.6 m, 11.6 m, and 16.1 m, respectively. Clearly, the BTG rockhead elevations have a
199 larger variability than that of the KF-OA interface elevation. The reason is that the BTG is older
200 than the two deposit formations and has undergone more tectonic events. The coordinates of the
201 boreholes and associated rockhead elevations at Site 3 are listed in Table A1 in the appendix while
202 those for the other two sites can be found in Qi et al. (2020a). Note that elevation rather than depth
203 is used to indicate the location of the geological interface because the depth parameter can be
204 affected by localized excavation activities and it may vary with time.
205 In the engineering practice of Singapore, the weathering degree of rock masses is classified
206 into six grades including residual soil (RS, Grade VI), completely weathered rock (CWR, Grade
207 V), highly weathered rock (HWR, Grade IV), moderately weathered rock (MWR, Grade III),
208 slightly weathered rock (SWR, Grade II) and fresh rock (FR, Grade I). The weathering grade of
209 the rock mass in Singapore is determined according to a British code (British Standard Committee
210 1999). The rock masses with weathering grades IV to VI are considered to be soils while those
211 with weathering grades I to III are considered to be rocks, as described in Shirlaw et al. (2000).

The rockhead is considered to be the top of the formations layers with weathering grades I to III. However, it should be noted that sometimes a thin layer (e.g., thickness < 2 m) is described to be MWR, SWR or FR, but overlies certain soil layers. This thin layer is likely to be a boulder and not considered to be a rock layer. In this study, the weathering grade information of the BTG and geological interface information is obtained from borehole logs in site investigation reports.

4. Spatial prediction of the location of geological interfaces

In this section, the accuracies of the MARS method, CRF method, and TPSI method in predicting the geological interface elevations are compared using a cross-validation procedure. Patterns of the predicted surfaces and the prediction intervals of the geological interface elevation evaluated by different methods are also compared. To obtain a comprehensive understanding of the performance of various methods, the comparisons are performed using borehole data from three sites in Singapore, as described in section 3. The borehole data in the three sites are discussed in subsections 4.1, 4.2, and 4.3, respectively. Note that the zonation method is only used in Sites 2 and 3 since the geological data at Site 1 have a relatively small variability and there are no major geological structures present at this site, which can significantly complicate the geological profiles.

4.1 Kallang Formation – Old Alluvium interface at Site 1

The KF-OA interface surfaces are firstly evaluated using all the KF-OA data to obtain an overall understanding of the KF-OA interface trend in the site. Afterward, the accuracies of various methods are compared through cross-validations.

4.1.1 Predicted KF-OA surface using all the data

The surfaces and curves of the KF – OA interface predicted by different methods using all the KF – OA data are plotted in Fig. 3. Since the MARS and CRF methods can evaluate the prediction uncertainty, the 95% prediction intervals of the KF – OA interface elevation for the cross-section,

235 y = 200 m are also plotted in Figs. 3(b) and (d). The 95% prediction interval is bounded by the
236 mean value ± 1.96 times the standard deviation. Note that for the CRF method, a model selection
237 using the Bayesian information criterion indicates that the optimal form of trend function, $T(x, y)$,
238 of the KF-OA interface elevation is a linear function of y as shown by

239 $$T(x, y) = \beta_0 + \beta_1 \times y \quad (2)$$

240 where β_0 and β_1 are regression coefficients; x and y are the coordinate values. A widely-used
241 separable single exponential is used to express the autocorrelation of the geological interface
242 elevation. The estimated random field parametric values are SoF_x = 99 m, SoF_y = 66.6 m,
243 standard deviation σ = 4.5 m, β_0 = -20.9 m, β_1= 1.64×10^{-02}. Besides, for the MARS method, the
244 spline functions for the predicted mean trend of the KF–OA interface, z and the standard deviation
245 of prediction are given by (Qi et al. 2020a)

246 $$z = -19.3 + 1.20 \times10^{-3} \times \max(0, 934.13-x) + 1.75 \times10^{-2} \times \max(0, x-934.13) - 2.53\times 10^{-2} \times$$
247 $$\max(0, 262.54-y) + 3.71 \times10^{-2} \times \max(0, y-262.54) + 1.09 \times10^{-4} \times \max(0, 619.17-x) \times \max(0,$$
248 $$262.54-y) + 2.82\times10^{-5} \times\max(0, x-619.17) \times \max(0, 262.54-y) \quad (3a)$$

249 $$\text{Standard deviation of prediction} = 5.27 - 5.50 \times 10^{-4} \times x - 3.29 \times 10^{-3} \times y \quad (3b)$$

250 For the thin-plate spline interpolation, the fitted surface is obtained using the MATLAB function
251 '*fit*' with the '*fitType*' parameter set to be '*thinplateinterp*'. From Fig. 3, the following phenomena
252 can be observed.

253 (1) The CRF method may underestimate the extreme values of the geological interface elevation.
254 The reason is that the CRF method is similar to a weighted average method and the predicted
255 value for a target point cannot be larger or smaller than the observed values within a
256 neighborhood of the target point. As shown in Figs. 3(c-f), the surfaces produced by both the
257 CRF and TPSI methods run across known data points. However, the surface for the former has

extreme values (i.e., peaks or valleys) located mainly at the borehole sites. In this regard, the CRF method cannot produce a realistic surface because it fails to capture potential peaks or valleys of the geological interface surface, which might pose a risk in underground constructions.

(2) The surface from the MARS method has less fluctuation and can show the spatial trend of the geological interface more clearly than those from the other two methods. As shown in Figs. 3(c-f), the surfaces and curves predicted by the CRF and TPSI methods have many oscillations. These oscillations are caused by the constraint that the surface has to run across all the known points. Consequently, one can easily see the trend of the geological interface from the surface or curve predicted by the MARS (see Fig. 3(a, b)), but cannot from those by the CRF and TPSI methods. Because of this, it may be easier to use the MARS method to impose some trend or shape constraints to assist the application of engineering judgement to the predicted surface or profile, as shown in Wood (1994), Abraham and Khadraoui (2015).

(3) The prediction interval produced by the MARS method well reflects the data density and geological complexity while that by the CRF method reflects the distance from a location to the nearest data point. As shown in Fig. 3(b), the width of the prediction interval from the MARS method generally decreases with an increasing x because of the relatively high density of data points on the right-hand side as well as the relatively complex trend on the left-hand side. By contrast, the CRF method provides a prediction interval with a width increasing rapidly from 0 at known borehole sites to a certain level at another site, the magnitude of which depends on the distance from the site to the nearest borehole. In this regard, the prediction interval of the MARS method is more useful to guide future site investigations as it directly

reflects the data density and geological complexity, which was also discussed in Qi et al. (2020a).

4.1.2 Comparison of the prediction accuracies of different methods

In this subsection, the overall prediction accuracies of various spatial prediction methods are compared using the cross-validation procedure described in Section 2. In total, 100 rounds of cross-validations are performed and in each round, 70% of data are randomly drawn as training data. The prediction accuracies for different methods are summarized in Table 1. For brevity, Table 1 only lists the results for 30 experiments. Since the MARS and CRF methods can quantify the uncertainty of the predictions and provide a prediction interval, the coverage percentage (CP) of the 95% prediction intervals for these two methods are also summarized in Table 1. Herein the coverage percentage is the percentage of the testing data with observed values of the KF-OA interface elevation covered by the prediction interval. The following phenomena can be observed.

(1) Both the MARS method and CRF method produce satisfactory prediction intervals in the sense that the coverage percentage of the prediction interval is close to the confidence level. As shown in the last row of Table 1, the average value of the coverage percentage is close to the confidence level, 95%. This consistency indicates that both methods can produce a prediction interval that reasonably reflects (neither overestimate nor underestimate) the uncertainty of geological interface elevations in unexplored areas.

(2) The MARS and CRF methods have similar prediction accuracies, and their accuracies are generally higher than the TPSI method. As shown in the last row of Table 1, the mean values of *RMSE* for the MARS and CRF methods are similar but lower than those of the TPSI method.

To obtain a clearer picture of the performances of various methods, three typical examples of the cross-validation cases are analyzed, including experiments 2, 5, and 21 in Table 1. Experiment 2 is a case where the TPSI is found to be inferior to the other two methods, while experiment 5 is a case where the MARS has a lower accuracy than the CRF method. Furthermore, experiment 21 illustrates a case where the MARS outperforms the CRF method in prediction accuracy. The three examples are plotted in Figs. 4-6, respectively. In each figure, the plan view of training and testing boreholes and the predicted surfaces and curves of the KF-OA interface are plotted. The following phenomena can be observed from Figs. 4-6 and Table 1.

(1) In most cases such as experiment 2 in Table 1, the MARS method and CRF method have higher accuracies than the TPSI. As shown in Fig. 4(b), the KF-OA interface curve for y = 339 m predicted by the TPSI method is farther away from the testing point (x, y) = (372 m, 339 m) than those by the MARS and CRF methods. The reason is that the TPSI uses data points in a relatively small neighborhood of a target point in spatial predictions. For example, in Fig. 4(a), the testing borehole at (x, y) = (372 m, 339 m) is surrounded by three training boreholes revealing KF-OA interface elevation of -10.3 m at (x, y) = (248 m, 340 m), -13.5 m at (x, y) = (333 m, 308 m), and -7.4 m at (x, y) = (452 m, 344 m). For the TPSI method, these three boreholes give rise to a dramatically increasing trend of the KF-OA interface along the y-direction in the local area. Consequently, the predicted elevation of the KF-OA interface at (x, y) = (372 m, 339 m) is much higher than the actual value (-22.6 m) (see Fig. 4(b)). By contrast, for the MARS and CRF methods, the spatial prediction of a target point is affected by boreholes in a larger neighborhood (see Figs. 4(c, d)). The reason is that the MARS essentially is a regression method (mean trend determined by all the data points in one spline piece) while the CRF method makes use of the prior mean trend inferred from all the boreholes. As shown

in Fig. 4(b), the KF-OA interface elevations at (x, y) = (372 m, 339 m) predicted by the MARS and CRF methods are closer to the actual value (-22.6 m) than that by the TPSI because neighboring boreholes on the left reveal a relatively deep KF-OA interface.

(2) Although the overall accuracies for the MARS and CRF methods are similar, the two methods still have some differences in individual cases. As shown in Fig. 5, the MARS method has larger prediction errors than the CRF method for two testing boreholes at the lower-left corner. The reason is that the area has erratic geological conditions (see Fig. 3(a)) and only two neighboring training boreholes reveal similar elevation of KF-OA interface as these testing boreholes. As a result, the MARS cannot correctly detect the trend of the KF-OA interface at the lower-left corner. As shown in Fig. 5(c), the spline contains only two pieces separated by y = 201 m. The spline piece with y < 201 m has a relatively low surface because the training boreholes in this piece such as several distant boreholes on the right-hand side generally have deep KF-OA interfaces. As a result, the KF-OA interface elevations at the lower-left corner are significantly underestimated by the MARS. By contrast, for the CRF method, the distant boreholes do not have so great influence on the spatial prediction as the predicted surface needs to run across the training data points close to the several testing boreholes (see Fig. 5(b, d)). The errors for these testing boreholes, hence, are relatively small for the CRF method.

On the contrary, if sufficient boreholes exist at the zone with highly variable geological conditions, the MARS method can automatically detect this geologically complex area by placing proper knots. This is demonstrated by the case shown in Fig. 6, which includes two more training boreholes at the lower-left corner area than the case in Fig. 5. As shown in Fig. 6(c), the MARS method places two knots at x = 694 m and y = 255 m, which separate the lower-left corner zone from the other zones. As a result, the trend of the KF-OA interface at

the lower-left corner can be reasonably detected and the MARS method produces a smaller prediction error than the CRF method (see Fig. 6(b, c, d)). Based on the analyses of the two cases in Figs. 5 and 6, it can be concluded that the MARS method has higher prediction accuracies than the CRF method when relatively sufficient data are available in the zone with erratic geological conditions.

4.2 Bukit Timah Granite rockhead at Site 2

This section investigates the spatial prediction of the BTG rockhead at Site 2 using the MARS and CRF method. These BTG data represent a more geologically complex condition than that in the last subsection. For the CRF method, a model selection using the Bayesian information criterion indicates that the optimal form of trend function of the BTG rockhead at this site is a constant. The random field parametric values estimated from the maximum likelihood estimation using all the data points are SoF_x = 84.3 m, SoF_y = 164.7 m, standard deviation σ = 10.2 m, mean β_0 = -21.3 m. Figs. 7(a, b, c) plot the fitted surfaces and curves of rockhead for the MARS and CRF methods. As shown in Fig. 7(a, c), the MARS method cannot capture the deep rockhead located around (x, y) = (300 m, 150 m). For example, the fitted curve of the BTG rockhead is more than 15 m higher than the observed value at (x, y) = (282 m, 166 m) (see Fig. 7(c)). The reasons are that only four boreholes reveal deep rockhead (i.e., elevation < - 43 m) around the location (x, y) = (300 m, 150 m) and these four boreholes are surrounded by boreholes revealing much shallower rockheads (see Fig. 1(b)). Ideally, two knots should be placed at $x \approx$ 300 m and $y \approx$ 150 m to capture the local deep rockhead. However, the MARS method fails to make a knot placement at $y \approx$ 150 m because the deep-rockhead data are so limited that the fitting error cannot be reduced significantly if a knot is placed around $y \approx$ 150 m. By contrast, the CRF method can well capture the local trend of rockhead (see Fig. 7(b)) because the predicted surface has to run across all the known data points.

For this site, the site investigation report indicates that some faults exist at the site based on the geological map but does not provide the strike and location information. Hence, zonations are performed to improve the performance of the MARS method. As shown in Fig. 1(e) and Fig. 7(d), three boreholes located around (x, y) = (300 m, 150 m) reveal significantly deep rockhead than the neighboring boreholes. Based on this observation, two zonation schemes that divide the investigated area into three zones are proposed, as shown in Figs. 7(d) and 7(e). In Fig. 7(d), the three zones are separated by the lines x = 260 m and y = 200 m (x > 260 m) while in Fig. 7(e), the three zones are separated by the lines x = 260 m and x = 325 m. These boundary lines are chosen because all can separate the deep-rockhead data from certain shallow-rockhead data. The predicted rockhead curves and surfaces are plotted in Figs. 7(c), 7(f), and 7(g), respectively. As shown, both schemes can detect the deep rockhead located around (x, y) = (300 m, 150 m), although the two produce significantly different surfaces in the area with x > 260 m. However, it is difficult to tell which scheme is better until additional boreholes are drilled around (x, y) = (300 m, 150 m).

Furthermore, 50 rounds of cross-validations are performed to evaluate the prediction accuracy of the two methods. In each round, 70% of data points are randomly drawn for training and the remainder is used for testing. Note that when a zonation is performed, spatial predictions are performed independently in each zone. The *RMSE*, *RMSRE* and CP of cross-validations for different methods are summarized in Table 2. For brevity, only the results for 30 cross-validation cases are listed. As shown, the CRF and TPSI methods have a higher prediction accuracy than the MARS method when no zonation is conducted. However, after zonation, the MARS method has a prediction accuracy similar to that of the CRF method and higher than that of the TPSI method, indicating that a zonation can improve the prediction accuracy of the MARS when limited data are available in a geologically complex area. Note that another zonation scheme containing two zones

394 separated by the line x = 260 m is also evaluated. This zonation scheme produces a mean *RMSE*
395 and *RMSRE* of 8.0 m and 1.02, respectively. This performance is better than the scheme with no
396 zonation but slightly worse than the two schemes with three zones. This result is expected because
397 the boundary line, x = 260 m separates the deep-rockhead data from the shallow-rockhead data on
398 the left-hand side but cannot from the shallow-rockhead data on the right-hand side or in the area
399 with y > 200 m. Zonation schemes with more (≥ 4) zones are not considered because a large
400 number of zones may induce too limited data in each zone. Furthermore, the average values of the
401 CP for the 95% confidence intervals produced by the MARS method are close to 95%, no matter
402 whether the zonation is performed, indicating the reasonableness of the confidence intervals
403 produced by the MARS method.

404 **4.3 Bukit Timah Granite rockhead at Site 3**

405 This section further investigates the performance of the MARS and CRF methods using the BTG
406 data at Site 3. The rockhead data at this site are sparser and have a larger variability than those at
407 Site 2 (see section 3). For the CRF method, a model selection using the Bayesian information
408 criterion indicates that the optimal form of trend function of the BTG rockhead elevation at this
409 site is a linear function of the coordinate x and y, given by

410 $$T(x, y) = \beta_0 + \beta_1 \times x + \beta_2 \times y \quad (4)$$

411 The random field parametric values estimated from the maximum likelihood estimation method
412 using all the data points are SoF_x = 296.6 m, SoF_y = 89.3 m, standard deviation σ = 11.1 m, β_0
413 = -18.0 m, β_1 = 1.05 ×10^{-1}, β_2 = -2.51 ×10^{-2}. Figs. 8(a, b, c) plot the fitted surfaces and curves of
414 rockhead for the MARS and CRF methods. As shown in Fig. 2(f), Figs. 8(a, c), the MARS method
415 cannot capture the relatively shallow rockhead located in the area with 280 m < x < 420 m, and
416 500 m < y < 600 m. For example, the residual of fitting for the point located at (x, y) = (293.6 m,

575.0 m) is larger than 25 m (see Fig. 8(c)). The reason for this large residual is that only three boreholes reveal relatively shallow rockhead in the area with 280 m < x < 420 m, and 500 m < y < 600 m (see Fig. 2(f) and 8(d)). Such limited data are not sufficient for the MARS method to detect the local trend. By contrast, the CRF method can capture the trend because the predicted surface runs through all the known data points.

However, the above-mentioned problem can still be resolved by performing a zonation. Fig. 8(d) plots a zonation scheme in which the three boreholes with shallow rockheads are separated from the deep-rockhead boreholes on the lower side. The resultant curve and surface of the rockhead predicted by the MARS are plotted in Figs. 8(c, e), respectively. As shown, the predicted curve and surface reasonably capture the rockhead trend in the local erratic area. The residual of fitting for the point located at (x, y) = (293.6 m, 575.0 m) is around 7 m, which is much smaller than the value (> 25 m) when no zonation is conducted (see Fig. 8(c)).

To explore the effect of zonation on the spatial predictions, 47 rounds of leave-one-out cross-validation are performed. Due to the limited data, only one data point is drawn as testing data while the remainder is set as training data in each round of cross-validations. The prediction errors for 30 rounds of cross-validations are summarized in Table 3. As shown by the average prediction errors shown in the last row in the table, the MARS method has a prediction error higher than the CRF method but lower than the TPSI method when no zonation is performed. Nevertheless, after zonation, the MARS method achieves a prediction accuracy similar to that of the CRF method but much higher than that of the TPSI method. These observations are similar to those for Site 2. This result further shows the capability of the MARS in dealing with complex geological conditions. Analyses of the individual cases are similar to those in section 4.1 and are not presented herein.

5 Summary and conclusions

This study compares three commonly used spatial prediction methods for predicting the location of the interface of geological formations in a two-dimensional space using borehole data from three sites in Singapore. The three methods are the multivariate adaptive regression spline method, conditional random field method, and thin-plate spline interpolation method, respectively. The interfaces studied are the interface between Kallang Formation and Old Alluvium for Site 1, the rockhead of the Bukit Timah Granite for Site 2 and Site 3. The prediction accuracies, patterns of predicted surface, and prediction uncertainties for various methods are evaluated. A zonation is proposed to improve the prediction accuracy of the multivariate adaptive regression spline method. The following conclusions can be drawn from the analyses.

(1) The TPSI method may produce a geological interface surface with undesirable oscillations because it uses data in a very small neighbourhood. The CRF method may underestimate the extreme values of geological interface elevation as the method is similar to the weighted average method and extreme values occur mainly at the known borehole sites. By contrast, the surface evaluated from the MARS clearly shows the spatial trend of the geological interface and it is also easier to implement engineering judgement or knowledge by imposing constraints on the trend and shape of the profile of geological interfaces. This implementation can be realized by combining the Bayesian method with the spline regression methods, which will be investigated in the future.

(2) Both the MARS and CRF methods provide a reasonable prediction interval of the geological interface elevation in the sense that the 95% prediction intervals produced by both methods can cover around 95% of testing data in cross-validation experiments. The width of the prediction interval from the CRF method depends mainly on the distance from the target location to the nearest borehole. By contrast, the width of the prediction interval from the

MARS method reflects the data density and geological complexity and can provide useful guidance for future site investigations to be conducted.

(3) In general, the MARS method has a prediction accuracy similar to the CRF method but higher than the TPSI method. In cases where a geologically complex area is occupied by limited data, the MARS method may have a lower prediction accuracy than the CRF method. However, this problem can be well resolved by a zonation to separate the geologically complex areas from the geologically more uniform areas. The zonation can be readily performed by visual inspection to identify areas with sharp variations of geological intervals and then placing partition lines between boreholes with distinct differences in the elevations of geological interfaces. After zonation, the MARS method can achieve a prediction accuracy similar to that of the CRF method.

Acknowledgments

This research is supported by the Singapore Ministry of National Development and the National Research Foundation, Prime Minister's Office under the Land and Liveability National Innovation Challenge (L2 NIC) Research Programme (Award No. L2NICCFP2-2015-1). Any opinions, findings, and conclusions or recommendations expressed in this material are those of the authors and do not reflect the views of the Singapore Ministry of National Development and National Research Foundation, Prime Minister's Office, Singapore.

References

Abraham, C., & Khadraoui, K. 2015. Bayesian regression with B-splines under combinations of shape constraints and smoothness properties. Statistica Neerlandica 69, 150-170.

Armstrong, R.W. 2012. Explanation of the BGS Subsurface Viewer. In: Buchroithner, M. (ed.) True-3D in Cartography: Autostereoscopic and Solid Visualisation of Geodata. Springer, Berlin, Heidelberg, 229-237.

Aswar, D.S., & Ullagaddi, P.B. 2017. An overview of 3-D geological modelling part II. Summary of major 3-d geological modelling methodologies. International Journal of Latest Engineering and Management Research, 2(11), 15–27.

British Standard Committee. 1999. BS 5930: 1999 Code of practice for site investigations. British Standards Institution, London.

Chiam, S.L., Wong, K.S., Tan, T.S., Ni, Q., Khoo, K.S. & Chu, J. 2003. The Old Alluvium. Workshop “Updating the Engineering Geology of Singapore" In Proceedings Underground Singapore 2003. NTU, Singapore, pp. 408-427.

Dasaka, S.M. & Zhang, L.M. 2012. Spatial variability of in situ weathered soil. Géotechnique, 62(5), 375-384, doi: 10.1680/geot.8.P.151.3786.

Deng, Z.-P., Li, D.-Q., Qi, X.-H., Cao, Z.-J. & Phoon, K.-K. 2017. Reliability evaluation of slope considering geological uncertainty and inherent variability of soil parameters. Computers and Geotechnics, **92**, 121-131, doi: https://doi.org/10.1016/j.compgeo.2017.07.020.

Duchon, J. 1977. Splines minimizing rotation-invariant semi-norms in Sobolev spaces. In: Schempp, W. & Zeller, K. (eds). Constructive Theory of Functions of Several Variables. Lecture Notes in Mathematics. Springer, Berlin, Heidelberg, 85-100.

Friedman, J.H. 1991. Multivariate Adaptive Regression Splines. Ann. Statist., 19(1), 1-67, doi: 10.1214/aos/1176347963.

Hastie, T., Tibshirani, R. & Friedman, J. 2008. The elements of statistical learning: data mining, inference and prediction. Second edition. Springer.

507 Harder, R.L., & Desmarais, R.N. 1972. Interpolation using surface splines. Journal of Aircraft,
508 9(2), 189-191
509 Huang, Y., Beck, J.L., Wu, S. & Li, H. 2014. Robust Bayesian compressive sensing for signals in
510 structural health monitoring. Computer-Aided Civil and Infrastructure Engineering, 29(3),
511 160-179.
512 Lark, R., Mathers, S., Thorpe, S., Arkley, S., Morgan, D. & Lawrence, D. 2013. A statistical
513 assessment of the uncertainty in a 3-D geological framework model. Proceedings of the
514 Geologists' Association, 124(6), 946-958.
515 Li, D.-Q., Qi, X.-H., Cao, Z.-J., Tang, X.-S., Phoon, K.-K. & Zhou, C.-B. 2016. Evaluating slope
516 stability uncertainty using coupled Markov chain. Computers and Geotechnics, **73**, 72-82,
517 doi: 10.1016/j.compgeo.2015.11.021.
518 Li, X.Y., Zhang, L.M. & Li, J.H. 2016. Using conditioned random field to characterize the
519 variability of geologic profiles. Journal of Geotechnical and Geoenvironmental Engineering,
520 142(4), 04015096, doi:10.1061/(ASCE)GT.1943-5606.0001428.
521 Li, S., Li, P., & Zhang, M. 2021. Analysis of additional stress for a curved shield tunnel. Tunnelling
522 and Underground Space Technology 107, 103675.
523 Lo, M.K. & Leung, Y.F. 2017. Probabilistic analyses of slopes and footings with spatially variable
524 soils considering cross-correlation and conditioned random field. Journal of Geotechnical and
525 Geoenvironmental Engineering, 143(9), 04017044, doi: 10.1061/(ASCE)GT.1943-
526 5606.0001720.
527 Mariethoz, G. & Caers, J. 2014. Multiple-point geostatistics: stochastic modeling with training
528 images. John Wiley & Sons.
529 MathWorks, I. 2014. Curve fitting toolbox™: user's guide. MathWorks.

Montoya-Noguera, S., Zhao, T., Hu, Y., Wang, Y., & Phoon, K. K. 2019. Simulation of non-stationary non-Gaussian random fields from sparse measurements using Bayesian compressive sampling and Karhunen-Loève expansion. Structural Safety, 79, 66-79.

Pitts, J. 1984. A review of geology and engineering geology in Singapore. Quarterly Journal of Engineering Geology and Hydrogeology, 17(2), 93-101, doi: 10.1144/gsl.qjeg.1984.017.02.02.

Qi, X.-H., Li, D.-Q., Phoon, K.-K., Cao, Z.-J. & Tang, X.-S. 2016. Simulation of geologic uncertainty using coupled Markov chain. Engineering Geology, **207**, 129-140, doi: 10.1016/j.enggeo.2016.04.017.

Qi, X.-H. & Liu, H.-X. 2019a. An improved global zonation method for geotechnical parameters. Engineering Geology, 248, 185-196, doi: 10.1016/j.enggeo.2018.11.013.

Qi, X.-H. & Liu, H.-X. 2019b. Estimation of autocorrelation distances for in-situ geotechnical properties using limited data. Structural Safety, 79, 26-38, doi: https://doi.org/10.1016/j.strusafe.2019.02.003.

Qi, X. H., Wang, H., Pan, X.-H., Chu, J. & Chiam, K. 2020a. Prediction of interfaces of geological formations using the multivariate adaptive regression spline method. Underground Space, accepted, doi: 10.1016/j.undsp.2020.02.006.

Qi, X.-H., Pan, X.-H., Chiam, K., Lim, Y.-S. & Lau, S.-G. 2020b. Comparative spatial predictions of the locations of soil-rock interface. Engineering Geology, 272, 105651, doi: 10.1016/j.enggeo.2020.105651.

Samui, P., Kim, D. & Viswanathan, R. 2015. Spatial variability of rock depth using adaptive neuro-fuzzy inference system (ANFIS) and multivariate adaptive regression spline (MARS). Environmental Earth Sciences, 73(8), 4265-4272, doi: 10.1007/s12665-014-3711-x.

553 Sharma, J.S., Chu, J. & Zhao, J. 1999. Geological and geotechnical features of Singapore: an
554 overview. Tunnelling and Underground Space Technology, 14(4), 419-431, doi:
555 10.1016/S0886-7798(00)00005-5.
556 Shirlaw, J.N., Hencher, S.R. & Zhao, J. 2000. Design and construction issues for excavation and
557 tunnelling in some tropically weathered rocks and soils. ISRM International Symposium.
558 International Society for Rock Mechanics and Rock Engineering.
559 Wang, H., Wellmann, J.F., Li, Z., Wang, X. & Liang, R.Y. 2017. A segmentation approach for
560 stochastic geological modeling using hidden Markov random fields. Mathematical
561 Geosciences, 49(2), 145-177, doi: 10.1007/s11004-016-9663-9.
562 Wang, X., Wang, H., Liang, R.Y., Zhu, H. & Di, H. 2018. A hidden Markov random field model
563 based approach for probabilistic site characterization using multiple cone penetration test data.
564 Structural Safety, 70, 128-138, doi: https://doi.org/10.1016/j.strusafe.2017.10.011.
565 Wang, Y. & Zhao, T. 2016. Interpretation of soil property profile from limited measurement data:
566 a compressive sampling perspective. Canadian Geotechnical Journal, 53(9), 1547-1559, doi:
567 10.1139/cgj-2015-0545.
568 Wang, Y. & Zhao, T. 2017. Statistical interpretation of soil property profiles from sparse data
569 using Bayesian compressive sampling. Géotechnique, 67(6), 523-536, doi:
570 10.1680/jgeot.16.P.143.
571 Wang, Y., Akeju, O.V. & Zhao, T. 2017. Interpolation of spatially varying but sparsely measured
572 geo-data: A comparative study. Engineering Geology, 231, 200-217, doi:
573 10.1016/j.enggeo.2017.10.019.

574 Wang, Y., Zhao, T., & Phoon, K. K. 2018. Direct simulation of random field samples from sparsely
575 measured geotechnical data with consideration of uncertainty in interpretation. Canadian
576 Geotechnical Journal, 55(6), 862-880.
577 Wang, Y., Zhao, T., Hu, Y., & Phoon, K. K. 2019. Simulation of random fields with trend from
578 sparse measurements without detrending. Journal of Engineering Mechanics, ASCE, 145(2),
579 04018130.
580 Wang, Y., Hu, Y., & Zhao, T. 2020. CPT-based subsurface soil classification and zonation in a
581 2D vertical cross-section using Bayesian compressive sampling. Canadian Geotechnical
582 Journal, https://doi.org/10.1139/cgj-2019-0131.
583 Wang, L., Wu, C., Gu, X., Liu, H., Mei, G, & Zhang, W. 2020. Probabilistic stability analysis of
584 earth dam slope under transient seepage using multivariate adaptive regression splines.
585 Bulletin of Engineering Geology and the Environment, DOI: 10.1007/s10064-020-01730-0.
586 Zhang, W. & Goh, A.T. 2016. Multivariate adaptive regression splines and neural network models
587 for prediction of pile drivability. Geoscience Frontiers, 7(1), 45-52.
588 Wood, S.N. 1994. Monotonic smoothing splines fitted by cross validation. SIAM Journal on
589 Scientific Computing 15, 1126-1133.
590 Zhang, W., Wu, C., Li, Y., Wang, L., & Samui, P. 2019. Assessment of pile drivability using
591 random forest regression and multivariate adaptive regression splines. Georisk: Assessment
592 and Management of Risk for Engineered Systems and Geohazards, DOI:
593 10.1080/17499518.2019.1674340.
594 Zhang, W.G., Li, H.R., Wu, C.Z., Li, Y.Q., Liu, Z.Q., & Liu, H.L 2020. Soft computing approach
595 for prediction of surface settlement induced by earth pressure balance shield tunneling,
596 Underground Space, DOI: 10.1016/j.undsp.2019.12.003.

597 Zhao, T., Hu, Y. & Wang, Y. 2018. Statistical interpretation of spatially varying 2D geo-data from
598 sparse measurements using Bayesian compressive sampling. Engineering Geology, 246, 162-
599 175, doi: 10.1016/j.enggeo.2018.09.022.
600 Zhao, T. & Wang, Y. 2020. Interpolation and stratification of multilayer soil property profile from
601 sparse measurements using machine learning methods. Engineering Geology, 265, 105430.
602 Zheng, H., Li, P., & Ma, G. 2021. Stability analysis of the middle soil pillar for asymmetric parallel
603 tunnels by using model testing and numerical simulations. Tunnelling and Underground
604 Space Technology 108, 103686.
605

Table 1 Prediction accuracies for the spatial prediction of the Kallang Formation – Old Alluvium interface elevation at Site 1

	MARS			CRF			TPSI	
Experiment	*RMSE* (m)	*RMSRE*	CP (%)	*RMSE* (m)	*RESRE*	CP (%)	*RMSE* (m)	*RMSRE*
1	5.17	0.61	98	4.50	0.43	89	5.23	0.39
2	4.25	0.19	93	4.44	0.20	89	5.19	0.24
3	3.99	0.17	93	4.13	0.19	96	5.81	0.28
4	4.75	0.20	96	4.53	0.20	89	5.47	0.24
5	5.47	0.59	93	4.95	0.52	93	5.83	0.42
6	5.33	0.61	91	5.17	0.55	89	4.98	0.31
7	4.60	0.50	93	4.60	0.47	93	4.09	0.32
8	4.50	0.21	96	3.87	0.18	93	5.39	0.29
9	4.13	0.24	93	4.33	0.24	91	5.35	0.31
10	4.82	0.55	89	4.60	0.48	91	5.03	0.34
11	3.51	0.20	98	3.94	0.21	96	4.70	0.27
12	4.43	0.23	100	3.87	0.20	100	4.17	0.24
13	4.87	0.23	89	4.32	0.19	87	5.58	0.28
14	4.39	0.40	96	4.39	0.46	98	4.05	0.32
15	4.90	0.56	96	4.43	0.49	93	5.31	0.41
16	4.55	0.23	93	4.26	0.24	93	5.80	0.33
17	4.43	0.46	96	4.64	0.45	89	5.52	0.39
18	4.50	0.46	91	4.57	0.44	91	5.80	0.43
19	3.95	0.20	98	4.11	0.22	93	5.94	0.34
20	4.46	0.21	93	4.46	0.21	89	5.35	0.24
21	3.94	0.43	98	4.28	0.47	96	4.37	0.34
22	3.57	0.17	100	3.73	0.18	98	4.32	0.22
23	4.30	0.21	98	4.31	0.21	98	4.92	0.28
24	3.75	0.19	98	3.67	0.18	96	4.73	0.24
25	4.51	0.40	91	4.67	0.40	89	5.10	0.34
26	4.25	0.20	98	4.31	0.21	96	6.46	0.35
27	5.02	0.56	96	4.56	0.51	96	4.29	0.35
28	3.39	0.18	100	3.68	0.20	100	5.69	0.32
29	4.54	0.47	98	4.53	0.44	91	5.77	0.39
30	4.07	0.20	96	3.72	0.17	100	5.21	0.28
Average	4.40	0.32	95	4.24	0.31	94	5.17	0.31

Note: the last row summarizes the average value for 100 experiments. For brevity, the table only lists the results for 30 experiments.

Table 2 Prediction accuracies for the spatial prediction of the Bukit Timah Granite rockhead elevation at Site 2

Experiment	CRF			MARS (no zonation)			MARS (zonation scheme 1)			MARS (zonation scheme 2)			TPSI	
	RMSE (m)	*RMSRE*	CP (%)	*RMSE* (m)	*RMSRE*	CP (%)	*RMSE* (m)	*RMSRE*	CP (%)	*RMSE* (m)	*RMSRE*	CP (%)	*RMSE* (m)	*RMSRE*
1	7.04	0.91	93	8.24	0.89	98	6.73	1.24	95	6.57	1.23	98	7.44	0.71
2	6.88	1.05	95	10.13	2.38	100	6.80	0.63	95	6.89	0.69	98	8.11	1.00
3	7.08	0.66	95	10.72	0.49	92	5.69	0.90	95	6.60	0.91	100	7.35	0.81
4	6.24	0.77	100	7.62	0.83	100	6.88	0.50	98	6.87	0.55	98	7.32	0.97
5	6.53	1.38	98	9.30	2.00	98	6.99	1.65	100	6.99	1.65	100	7.57	1.56
6	5.65	0.64	100	7.98	1.65	100	6.18	0.46	98	7.54	0.48	98	6.82	0.90
7	7.40	0.88	90	9.30	1.72	98	7.09	0.78	93	8.29	0.93	88	8.27	0.86
8	6.70	1.38	98	9.30	2.22	98	8.35	2.14	93	9.27	2.15	95	6.93	1.19
9	7.49	1.09	93	9.36	1.27	98	6.42	1.14	100	6.95	1.14	100	8.17	1.05
10	8.87	0.90	93	10.13	1.38	95	6.44	1.32	98	8.49	1.33	98	10.08	0.71
11	6.31	0.28	98	8.51	0.50	98	6.61	0.32	95	6.99	0.49	83	7.94	0.36
12	7.83	0.33	93	10.22	0.35	98	8.29	0.33	93	8.51	0.33	95	6.10	0.30
13	7.10	1.13	95	9.39	1.08	100	8.83	0.93	85	8.81	0.94	90	8.09	0.91
14	7.40	0.68	95	10.30	0.80	92	10.05	0.88	93	8.32	0.79	95	9.44	0.88
15	7.37	1.15	98	7.65	0.71	100	6.42	0.60	95	7.76	0.64	93	8.50	0.92
16	7.56	0.95	95	8.84	1.68	100	7.45	0.86	93	7.26	0.86	100	9.33	0.91
17	6.00	1.29	100	9.49	1.85	100	7.79	2.22	98	6.26	1.40	98	6.15	1.54
18	8.30	0.77	95	11.48	1.33	95	8.14	1.00	98	8.24	1.00	95	10.13	1.08
19	7.42	1.29	95	10.83	2.04	95	9.61	1.97	98	9.03	1.68	95	8.19	0.83
20	8.36	0.78	85	10.28	1.11	95	8.16	1.08	88	6.73	1.03	95	10.05	0.96
21	5.51	0.74	100	9.39	2.71	95	7.14	1.54	100	6.75	1.54	98	8.32	1.00
22	8.01	0.40	90	8.99	0.72	100	8.26	0.45	90	7.30	0.35	90	10.21	0.55
23	7.00	0.82	95	9.29	2.43	98	7.86	1.34	95	6.97	1.33	95	8.31	0.94
24	6.91	0.62	95	9.19	1.72	100	7.42	1.79	93	8.62	1.80	98	8.18	0.85
25	7.27	0.70	95	9.11	1.37	100	6.00	1.00	98	9.40	1.16	100	8.01	0.94
26	7.19	2.12	93	6.07	1.25	100	7.02	1.72	98	7.69	1.98	95	7.35	1.68
27	5.67	0.76	100	8.74	2.31	100	6.75	0.85	100	7.41	1.27	98	7.44	1.31
28	5.03	0.82	100	8.52	0.77	100	6.19	0.77	98	7.77	0.85	98	7.14	0.83
29	7.96	0.51	90	9.38	1.20	95	8.52	0.99	98	8.48	0.99	93	9.30	0.44
30	7.76	1.27	93	8.24	1.64	98	6.62	1.19	93	7.65	1.19	98	8.04	0.55
Average	7.14	0.91	95	9.22	1.47	98	7.31	1.02	95	7.59	1.05	96	8.18	0.92

Note: the last row summarizes the average value for 50 experiments. For brevity, the table only lists the results for 30 experiments.

Table 3 Prediction accuracies for the spatial prediction of the Bukit Timah Granite rockhead elevation at Site 3

Experi-ment	CRF		MARS (no zonation)		MARS (zonation)		TPSI	
	RMSE (m)	*RMSRE*	*RMSE* (m)	*RMSRE*	*RMSE* (m)	*RMSRE*	*RMSE* (m)	*RMSRE*
1	13.83	0.60	8.28	0.36	10.01	0.44	20.05	0.87
2	16.69	2.26	33.37	4.51	27.63	3.73	31.74	4.29
3	12.51	0.27	7.91	0.17	6.63	0.14	6.37	0.14
4	1.14	0.03	1.70	0.05	13.17	0.36	11.26	0.31
5	1.20	0.05	0.41	0.02	2.49	0.10	10.42	0.42
6	7.17	0.56	5.49	0.43	3.65	0.28	8.89	0.69
7	8.80	0.40	8.82	0.40	1.95	0.09	6.58	0.30
8	15.20	0.31	10.80	0.22	8.34	0.17	13.78	0.28
9	3.52	0.09	4.77	0.12	2.11	0.05	10.33	0.26
10	6.94	0.24	2.03	0.07	6.96	0.24	6.04	0.21
11	2.79	0.17	22.72	1.38	5.04	0.31	7.60	0.46
12	6.43	0.19	6.09	0.18	4.37	0.13	13.39	0.39
13	11.04	0.24	13.63	0.30	1.25	0.03	8.71	0.19
14	17.72	0.79	10.90	0.48	22.85	1.02	8.47	0.38
15	0.01	0.00	1.78	0.05	4.36	0.11	13.91	0.36
16	14.70	0.33	11.36	0.25	6.18	0.14	7.59	0.17
17	1.40	0.06	5.65	0.23	7.90	0.32	6.81	0.28
18	7.00	0.25	14.90	0.52	10.22	0.36	3.11	0.11
19	9.70	0.26	6.20	0.17	10.44	0.28	6.84	0.18
20	11.26	0.36	5.43	0.17	7.33	0.23	6.25	0.20
21	11.19	0.25	8.08	0.18	14.39	0.33	19.04	0.43
22	12.35	0.54	27.39	1.19	0.02	0.00	25.01	1.09
23	22.83	1.25	29.93	1.64	29.87	1.63	32.54	1.78
24	2.58	0.07	10.10	0.26	19.59	0.51	7.85	0.21
25	7.73	0.17	10.34	0.23	6.93	0.15	6.17	0.14
26	8.27	0.31	7.90	0.29	8.89	0.33	14.74	0.55
27	17.23	0.38	14.21	0.31	20.26	0.45	21.87	0.48
28	22.02	1.30	15.15	0.89	11.53	0.68	27.60	1.62
29	10.37	0.51	0.30	0.01	12.72	0.62	12.86	0.63
30	1.11	0.04	6.57	0.21	1.24	0.04	13.88	0.44
Aver-age	8.77	0.36	9.83	0.45	9.03	0.40	12.12	0.53

Note: the last row summarizes the average value for 47 experiments. For brevity, the table only lists the results for 30 experiments.

Caption of figures

Fig. 1 Flowchart of zonation for the MARS method

Fig. 2 Geological profiles of cross-sections and borehole data at the three sites

Fig. 3 Kallang Formation –Old Alluvium interface elevation predicted by different methods using all the data at Site 1

Fig. 4 A case where the MARS and CRF methods outperform the TPSI (cross-validation experiment 2 in Table 1)

Fig. 5 A case where the CRF method outperforms the MARS method (cross-validation experiment 5 in Table 1)

Fig. 6 A case where the MARS method outperforms the CRF method (cross-validation experiment 21 in Table 1)

Fig. 7 Bukit Timah Granite rockhead predicted by different methods using all the data at Site 2

Fig. 8 Bukit Timah Granite rockhead predicted by different methods using all the data at Site 3

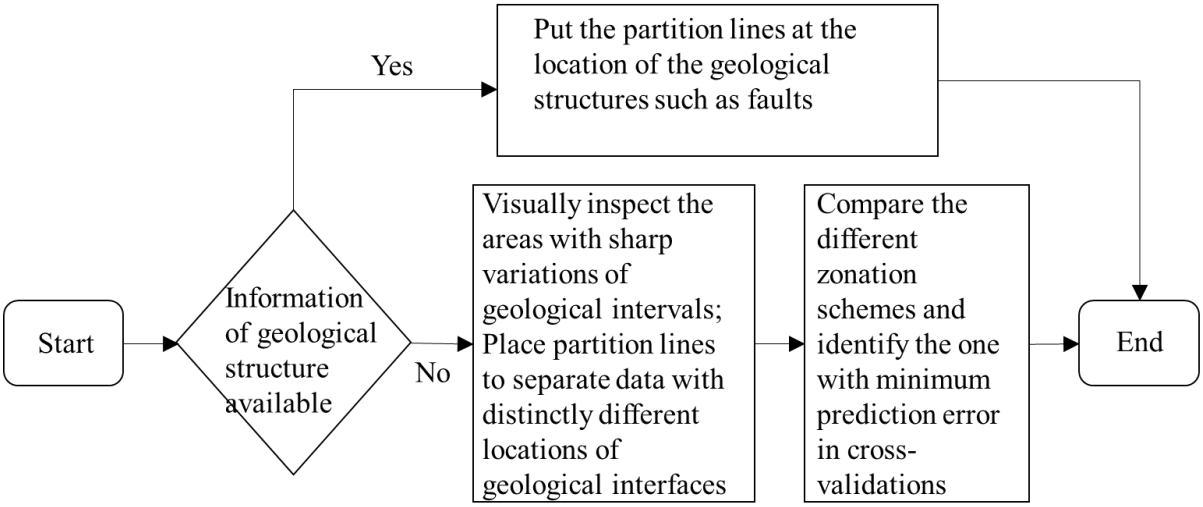

Fig. 1 Flowchart of zonation for the MARS method

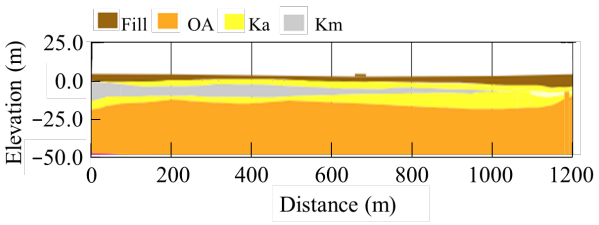

(a) Geological profile for a cross-section at Site 1

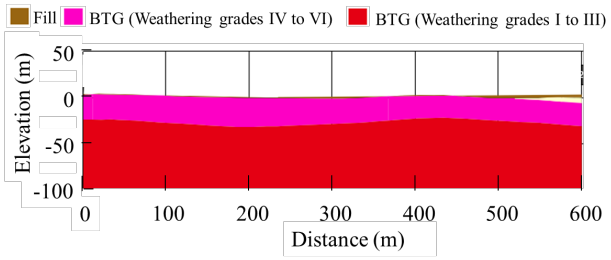

(b) Geological profile for a cross-section at Site 2

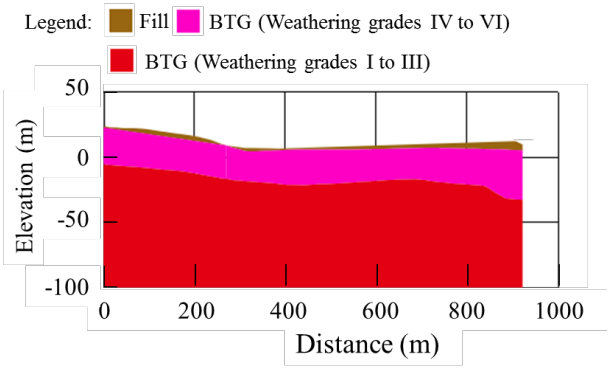

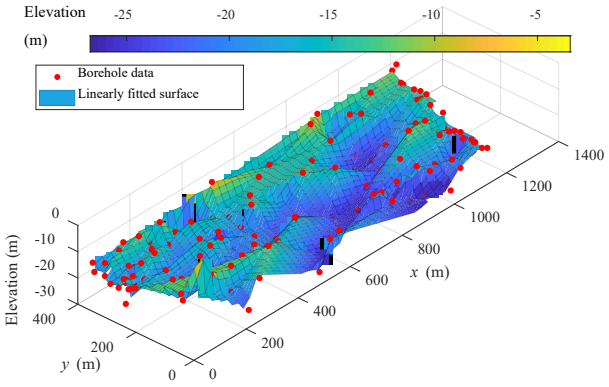

(c) Geological profile for a cross-section at Site 3 (d) Kallang Formation – Old Alluvium interface data at Site 1

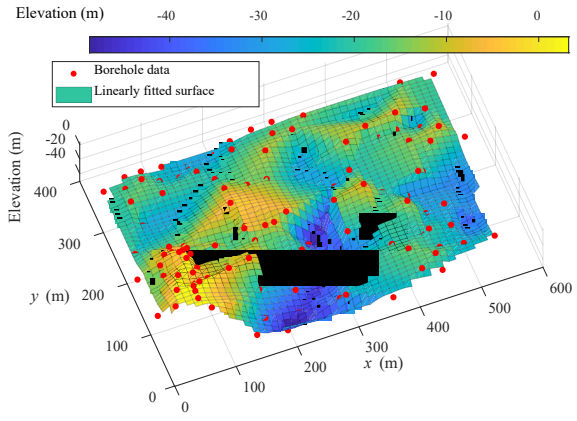

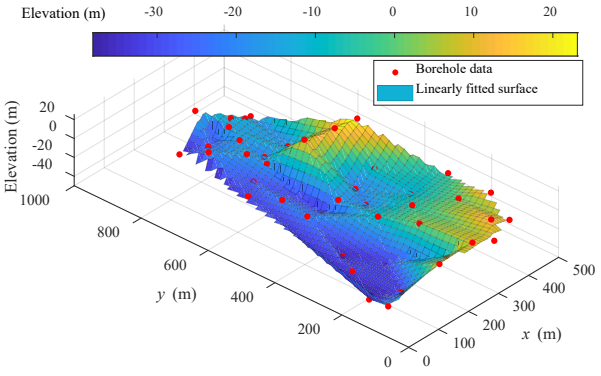

(e) Rockhead data of Bukit Timah Granite at Site 2 (f) Rockhead data of Bukit Timah Granite at Site 3

Fig. 2 Geological profiles of cross-sections and borehole data at the three sites

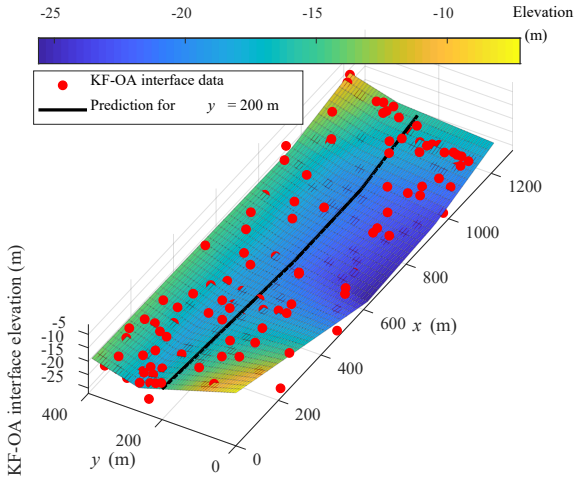

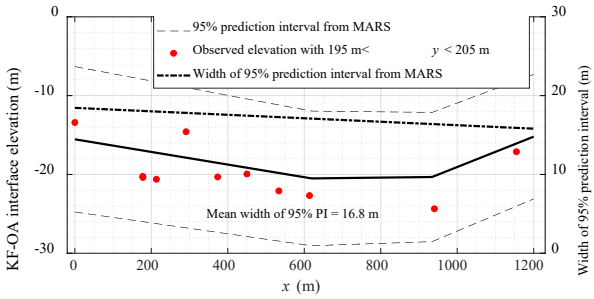

(a) Surface of KF-OA interface predicted by MARS (b) Predicted KF-OA interface elevation for $y = 200$ m (MARS)

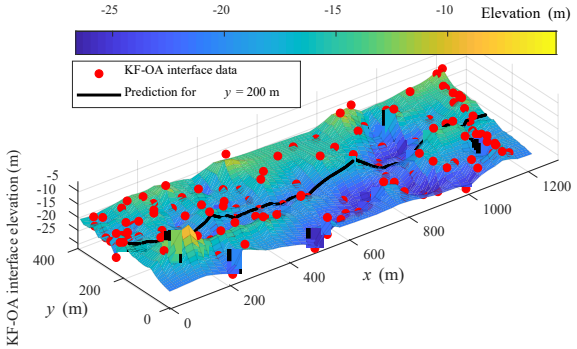

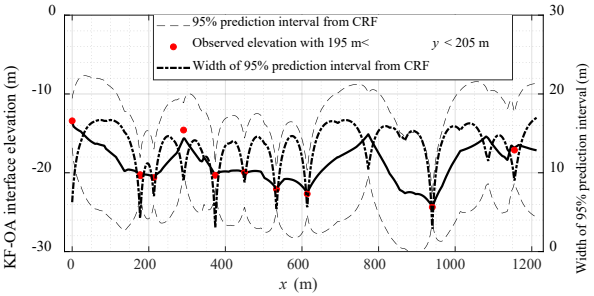

(c) Surface of KF-OA interface predicted by CRF (d) Predicted KF-OA interface elevation for $y = 200$ m (CRF)

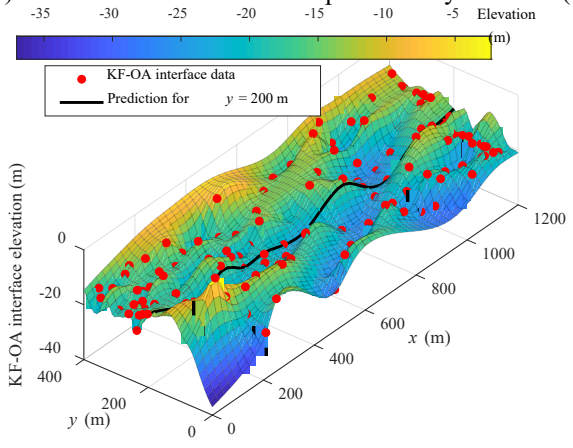

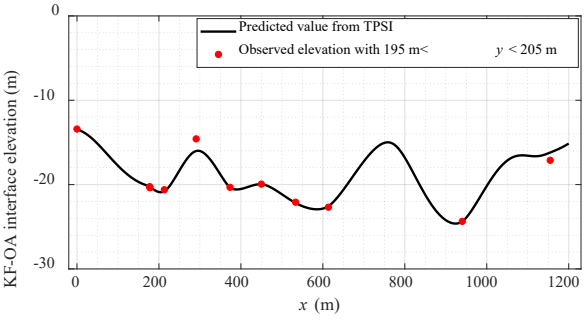

(e) Surface of KF-OA interface predicted by TPSI (f) Predicted KF-OA interface elevation for $y = 200$ m (TPSI)

Fig. 3 Kallang Formation –Old Alluvium interface elevation predicted by different methods using all the data at Site 1

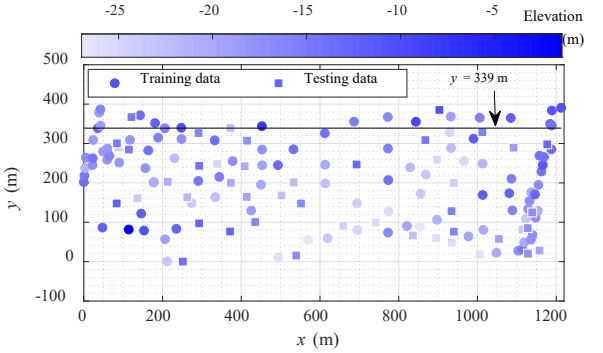

(a) Plan view of boreholes

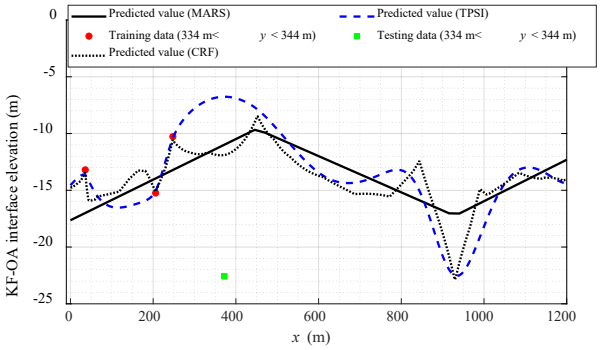

(b) Predicted curve of KF-OA interface for y = 339 m

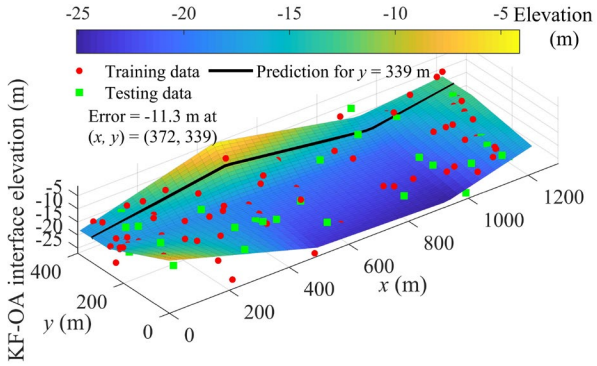

(c) Surface predicted by the MARS method

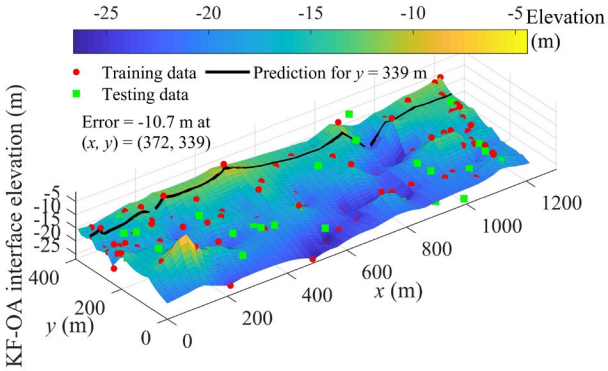

(d) Surface predicted by the CRF

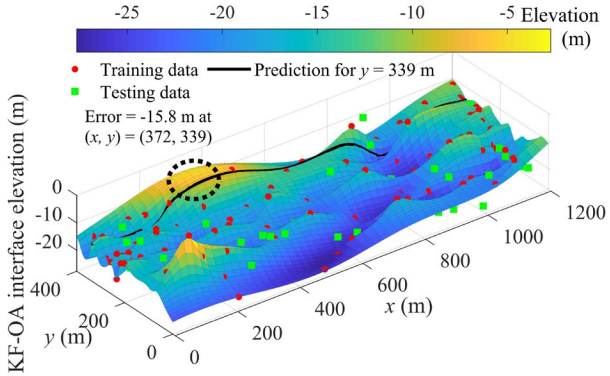

(e) Surface predicted by the TPSI Note: error = actual value – predicted value

Fig. 4 A case where MARS and CRF methods outperform TPSI (cross-validation experiment 2 in Table 1)

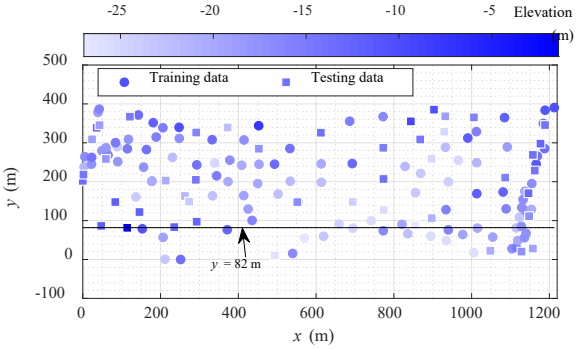

(a) Plan view of boreholes

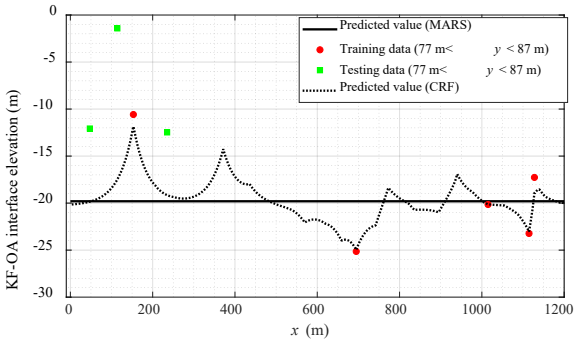

(b) Predicted curve of KF-OA interface for y = 82 m

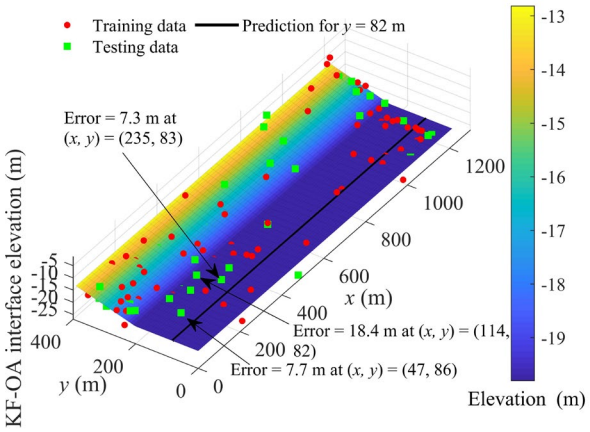

(c) Surface predicted by the MARS

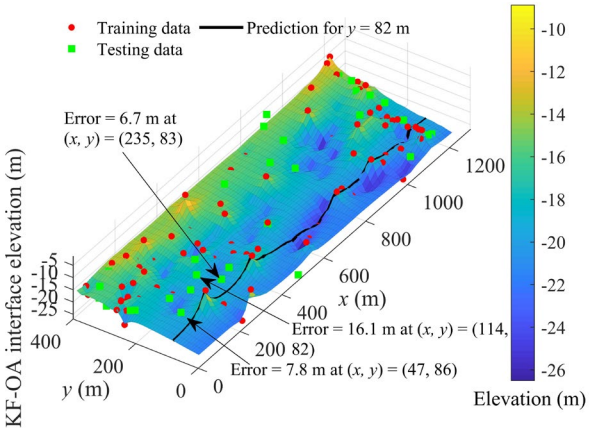

(d) Surface predicted by the CRF

(Note: error = actual value – predicted value)

Fig. 5 A case where CRF method outperforms MARS method (cross-validation experiment 5 in Table 1)

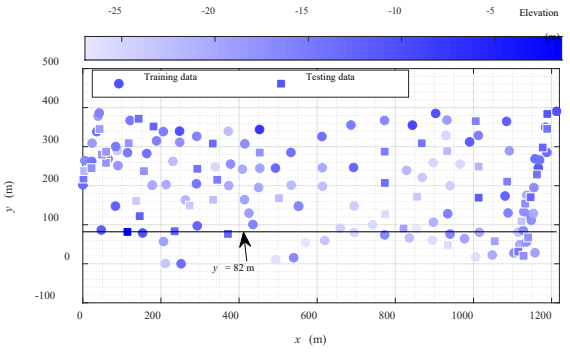

(a) Plan view of boreholes

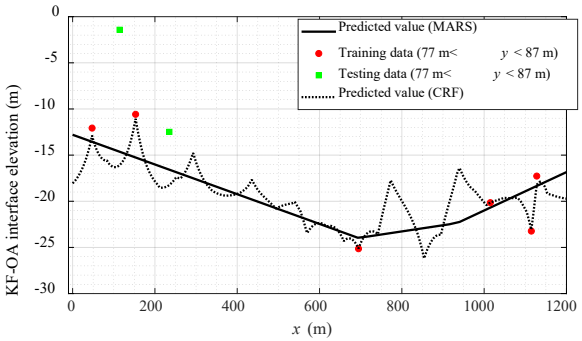

(b) Predicted curve of KF-OA interface for y = 82 m

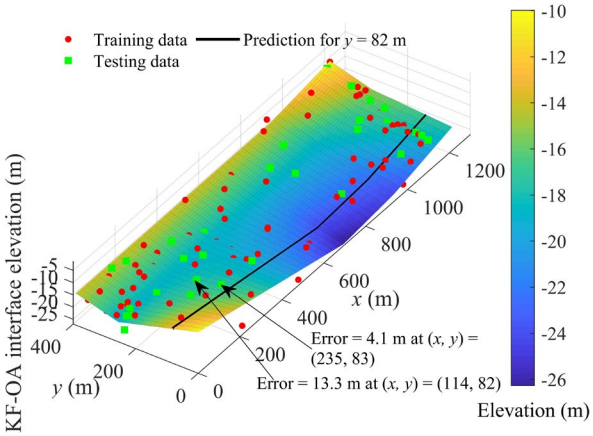

(c) Surface predicted by the MARS

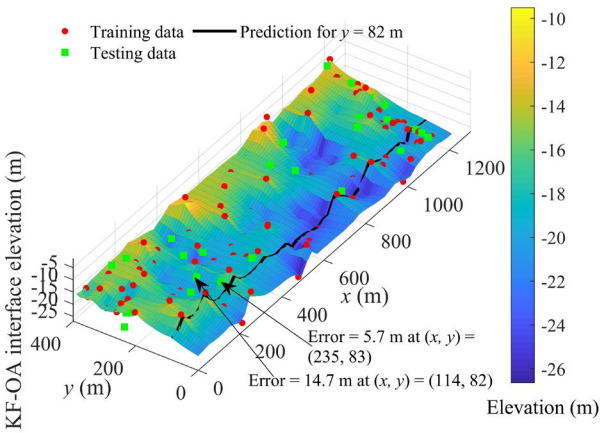

(d) Surface predicted by the CRF

(Note: error = actual value – predicted value)

Fig. 6 A case where MARS method outperforms CRF method (cross-validation experiment 21 in Table 1)

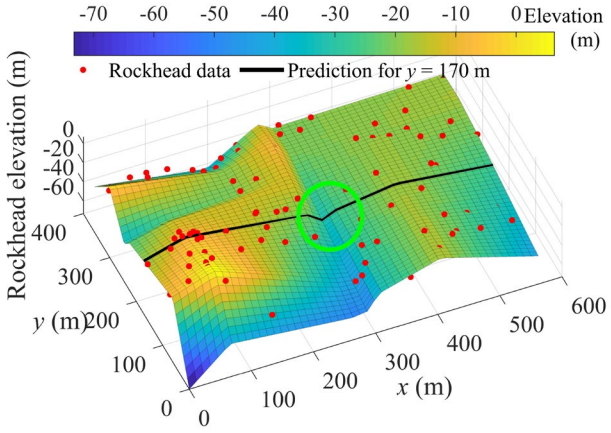

(a) Surface of rockhead predicted by MARS

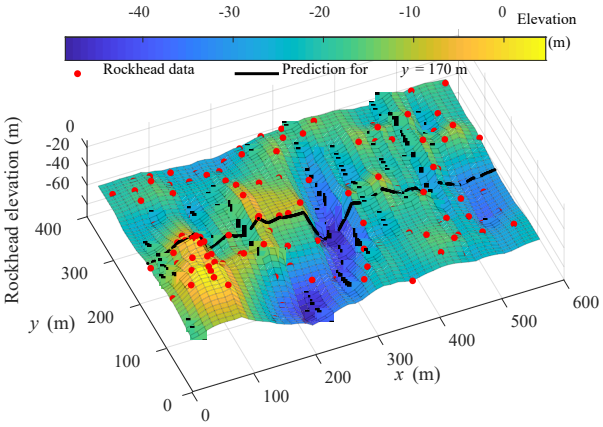

(b) Surface of rockhead predicted by CRF

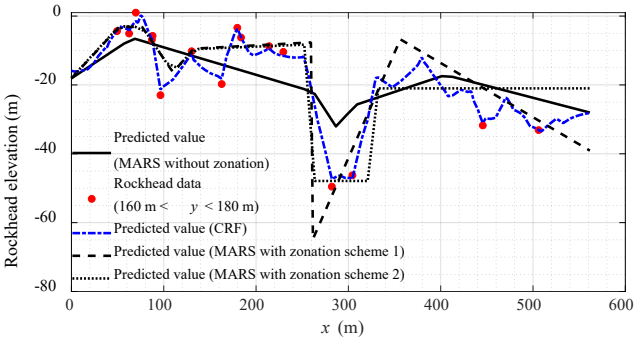

(c) Predicted curve of rockhead interface for y = 170 m

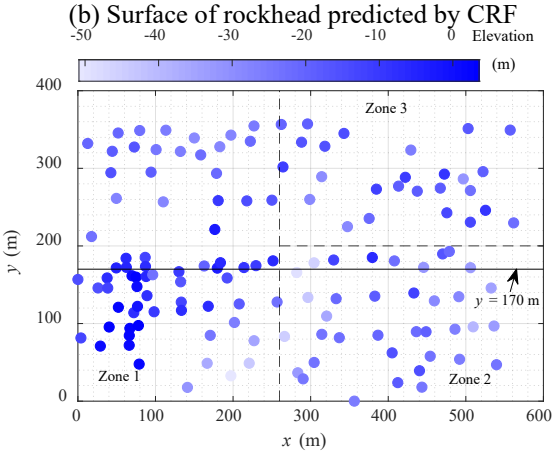

(d) A zonation of borehole data (scheme 1)

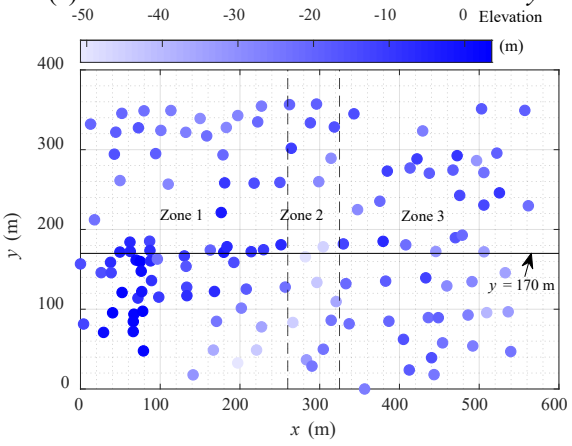

(e) A zonation of borehole data (scheme 2)

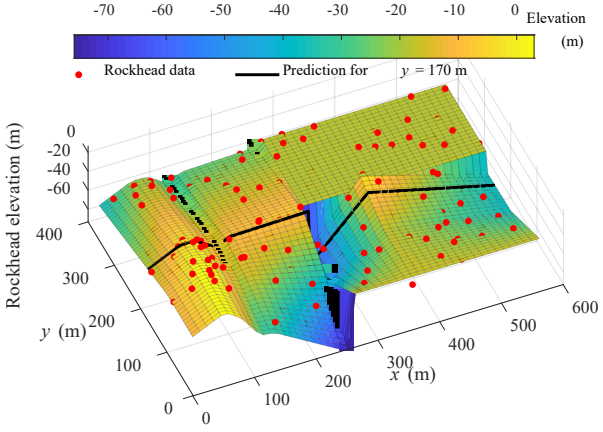

(f) Surface of rockhead predicted by MARS (zonation scheme 1)

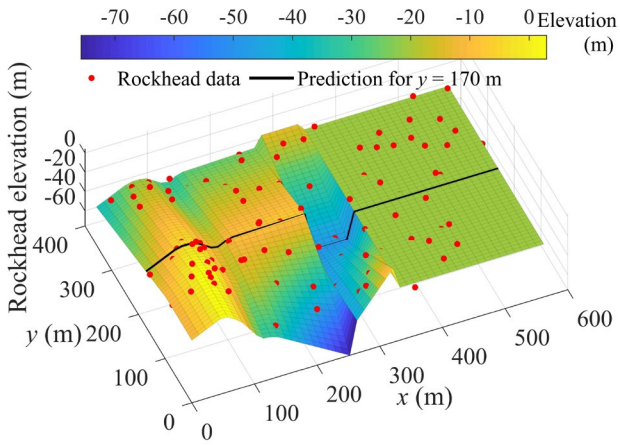

(g) Surface of rockhead predicted by MARS (zonation scheme 2)

Fig. 7 Bukit Timah Granite rockhead predicted by different methods using all the data at Site 2

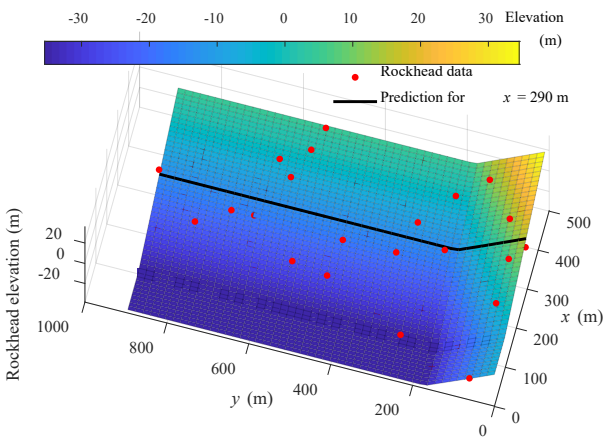

(a) Surface of rockhead predicted by MARS

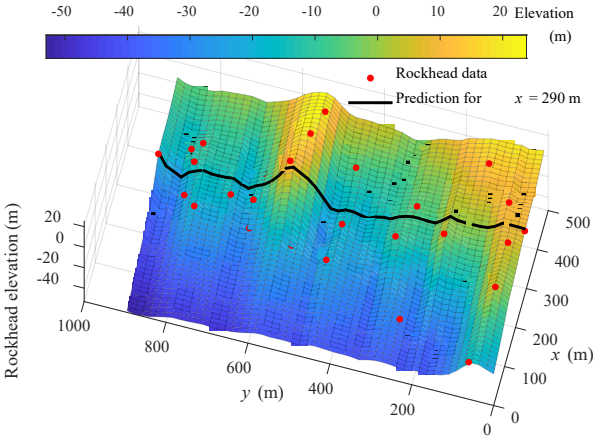

(b) Surface of rockhead predicted by CRF

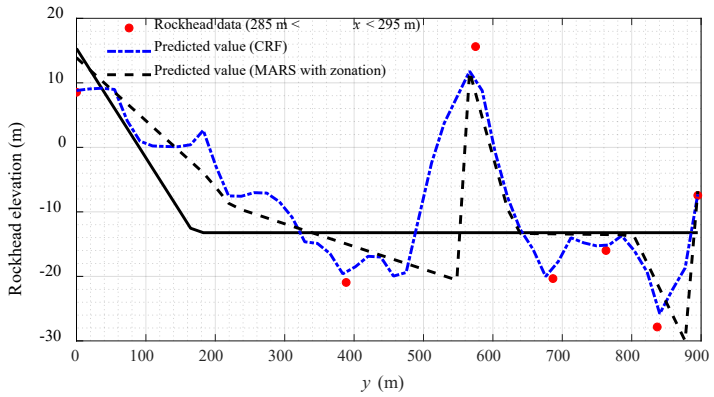

(c) Predicted curve of rockhead interface for x = 290 m

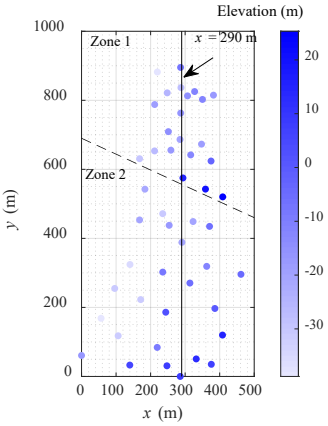

(d) A zonation of borehole data

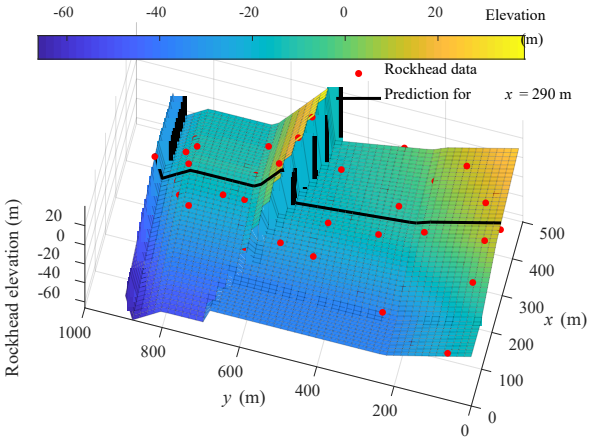

(e) Surface of rockhead predicted by MARS (zonation)

Fig. 8 Bukit Timah Granite rockhead predicted by different methods using all the data at Site 3

Appendix

The coordinates (x, y) and rockhead elevation (Ele) of the Bukit Timah Granite at Site 3 are summarized in Table A1.

Table A1 Borehole data used for spatial predictions at Site 3

x (m)	y (m)	Ele (m)	x (m)	y (m)	Ele (m)	x (m)	y (m)	Ele (m)	x (m)	y (m)	Ele (m)
0.0	60.8	-16.9	56.6	168.5	-38.8	347.4	673.0	-18.5	316.1	641.8	-12.1
139.7	32.9	6.1	243.8	186.1	2.9	211.8	787.8	-18.8	248.1	821.6	-25.4
140.2	324.3	-35.5	96.1	254.9	-31.3	219.5	882.0	-38.5	285.8	0.0	8.5
375.0	624.1	-2.8	171.3	222.7	-31.4	286.8	895.2	-7.5	408.2	119.9	15.6
287.2	762.9	-16.0	313.8	270.5	-5.5	375.8	35.2	7.5	461.7	295.8	-4.2
332.1	50.8	13.5	362.4	318.9	-11.6	370.7	434.7	-6.0	408.8	520.2	25.3
386.1	196.9	0.3	290.7	388.6	-20.9	106.0	117.8	-31.8	287.9	836.8	-27.8
235.0	471.6	-30.9	168.1	453.4	-20.8	235.2	302.3	-8.1	306.9	812.9	-14.3
285.1	686.5	-20.3	323.0	448.8	-20.6	253.8	437.8	-17.1	327.5	825.4	-11.2
251.4	709.2	-14.7	358.9	542.7	20.7	183.6	542.6	-21.7	350.2	802.5	-11.7
247.3	30.8	8.7	293.6	575.0	15.6	211.5	653.4	-26.7	382.0	814.9	-17.6
219.1	84.1	-9.2	168.1	630.8	-30.0	258.7	655.5	-17.1			